Acta Cryst E CRYSTALLOGRAPHIC COMMUNICATIONS

ISSN 2056-9890

Crystal growth, structure elucidation and CHARDI/BVS investigations of β-KCoFe(PO$_4$)$_2$

Adam Bouraima,[a,b]* Said Ouaatta,[a] Jamal Khmiyas,[a] Jean Jacques Anguilè,[b] Thomas Makani,[b] Abderrazzak Assani,[a] Mohamed Saadi[a] and Lahcen El Ammari[a]

[a]Laboratoire de Chimie Appliquée des Matériaux, Centre des Sciences des Matériaux, Faculty of Science, Mohammed V University in Rabat, Avenue Ibn Batouta, BP 1014, Rabat, Morocco, and [b]Laboratoire de Chimie des Matériaux Inorganiques, Faculté des Sciences, Département de Chimie, Université des Sciences et Techniques de Masuku, BP 943, Franceville, Gabon. *Correspondence e-mail: bouraima_adam@yahoo.com

Received 2 May 2022
Accepted 23 June 2022

Edited by M. Weil, Vienna University of Technology, Austria

Keywords: crystal structure; phosphate; zeolite-*ABW*; isotypism.

CCDC reference: 2181684

Supporting information: this article has supporting information at journals.iucr.org/e

Single crystals of β-KCoFe(PO$_4$)$_2$, potassium cobalt(II) iron(III) bis(orthophosphate), were grown from the melt under atmospheric conditions. This phosphate crystallizes isotypically with KZnFe(PO$_4$)$_2$ in space group $C2/c$, adopting a zeolite-*ABW* type of structure. The structure of the present phosphate is distinguished by an occupational disorder of the two transition-metal sites with ratios Fe:Co of 0.5725:0.4275 for the first and 0.4275:0.5725 for the second site. In the crystal structure, PO$_4$ and (Co,Fe)O$_4$ tetrahedra are linked through vertices to form elliptical rings with the sequence *DDDDUUUU* of up (*U*) and down (*D*) pointing vertices. Each eight-membered ring is surrounded by four other rings of the same type, delimiting interstices with rectangular shape. This arrangement leads to the formation of $[(Co/Fe)(PO_4)]^-_\infty$ sheets parallel to (001). Stacking of the sheets into a three-dimensional framework results in the formation of two types of channels. The first one is occupied by potassium cations, whereas the second one remains vacant. Calculations of bond-valence sums and charge distribution were used to confirm the structure model.

1. Chemical context

Transition-metal (*TM*) phosphates have been widely studied as potential candidates for various applications such as catalysis (Bautista *et al.*, 2007), ion exchange (Szirtes *et al.*, 2007), electrochemistry (Trad *et al.*, 2010) or as magnetic materials (Ofer *et al.*, 2012). In this context, zinc phosphates are of interest because the Zn^{2+} cation with its d^{10} electronic configuration is susceptible to strong polarization and thus can be used to design new non-linear optical (NLO) materials (Shen *et al.*, 2016). In the family of transition-metal phosphate compounds, the anionic network is formed from PO$_4$ tetrahedra bonded to different types of coordination polyhedra of the form [*TM*O$_n$] (n = 4, 5 and 6), leading to a wide variety of crystal structure types such as NaZnAl(PO$_4$)$_2$ (Yakubovich *et al.*, 2019). The structural diversity is mainly associated with the ability of *TM* cations to adopt different oxidation states with various types of coordination polyhedra (Moore & Ito, 1979; Hatert *et al.*, 2004).

It is in this context that our research team was involved with investigations of new phosphates with A^{I}, M^{II} and M^{III} cations where A is an alkali metal, and M^{II} and M^{III} are bivalent and trivalent cations, respectively. For example, $Na_2Co_2Fe(PO_4)_3$ (Bouraima *et al.*, 2015) and NaCuIn(PO$_4$)$_2$ (Benhsina *et al.*, 2020) are among the recently studied compounds. The present

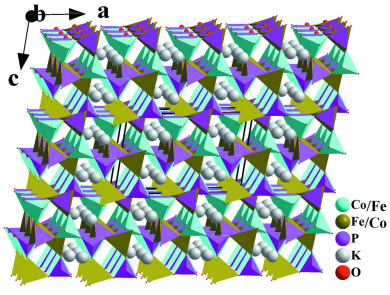

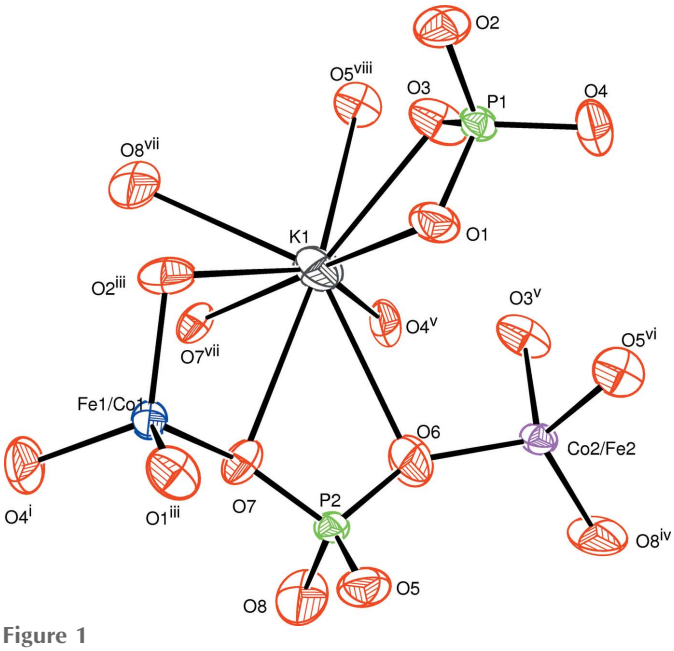

Figure 1
The principal building units in the crystal structure of β-KCoFe(PO$_4$)$_2$. Displacement ellipsoids are drawn at the 50% probability level. [Symmetry codes: (i) x, y, $z+1$; (ii) x, $-y$, $z+\frac{1}{2}$; (iii) $-x+1$, y, $-z+\frac{1}{2}$; (iv) $-x$, y, $-z+\frac{1}{2}$; (v) $-x+\frac{1}{2}$, $-y+\frac{1}{2}$, $-z$; (vi) x, $-y$, $z-\frac{1}{2}$; (vii) $-x+\frac{1}{2}$, $-y+\frac{1}{2}$, $-z+1$; (viii) $-x+\frac{1}{2}$, $y+\frac{1}{2}$, $-z+\frac{1}{2}$.]

work is devoted to synthesis and crystal structure analysis of β-KCoFe(PO$_4$)$_2$, a new compound in the family of transition-metal phosphates.

2. Structural commentary

The title compound crystallizes isotypically with KZnFe(PO$_4$)$_2$ (Badri *et al.*, 2015). The principal building units of β-KCoFe(PO$_4$)$_2$ are shown in Fig. 1, revealing that three types of more or less distorted tetrahedra build up the framework structure. The two *TM* sites are characterized by partial disorder (see *Refinement*) with (Fe/Co)1—O distances varying between 1.877 (2) and 1.900 (2) Å and (Co/Fe)2—O distances between 1.881 (2) and 1.927 (2) Å. The two PO$_4$ tetrahedra are more regular with the P—O bonds lengths between 1.5172 (19) and 1.5306 (19) Å for P1O$_4$ and 1.509 (2) and 1.533 (2) Å for P2O$_4$.

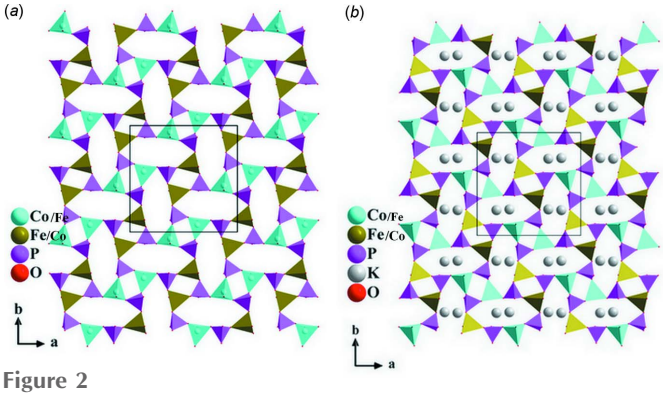

Figure 2
(*a*) A (001) layer at $z \simeq 0$ and (*b*) at $z \simeq 0.5$, resulting from vertex-sharing between *TM*O$_4$ and PO$_4$ tetrahedra. Rings formed by eight corner-sharing tetrahedra according to the sequence *DDDDUUUU* are shown on the left.

Table 1
CHARDI and BVS analysis for the cations in the title compound.

$q_{(i)}$ = formal oxidation number; sof$_{(i)}$ = site occupation factor; CN$_{(i)}$ = classical coordination number; $Q_{(i)}$ = calculated charge; $V_{(i)}$ = calculated valence; ECoN$_{(i)}$ = effective coordination number.

Cation	$q_{(i)}\times$sof$_{(i)}$	CN$_{(i)}$	ECoN$_{(i)}$	$V_{(i)}$	$Q_{(i)}$	$q_{(i)}/Q_{(i)}$
(Fe/Co)1	2.57	4	4.00	2.48	2.57	1.00
(Fe/Co)2	2.43	4	3.99	2.27	2.43	1.00
K1	1.00	9	8.71	0.94	0.99	1.00
P1	5.00	4	4.00	5.14	5.00	1.00
P2	5.00	4	3.99	5.15	5.01	1.01

The three different types of tetrahedra are linked through vertices to form ellipse-shaped rings with the sequence *DDDDUUUU* of up (*U*) and down (*D*) pointing vertices, as shown in Fig. 2. Each eight-membered ring is surrounded by four other rings of the same type, delimiting two interstices with rectangular shape constituted by two PO$_4$ and two (Fe/Co)1O$_4$ tetrahedra or two PO$_4$ and two (Co/Fe)2O$_4$ tetrahedra. This assembly leads to the formation of $[(Co/Fe)(PO_4)]^-_\infty$ sheets extending parallel to (001) at $z = 0, \frac{1}{2}$. Stacking of these sheets along [001] leads to the formation of a three-dimensional framework structure with two types of channels. The first one is occupied by potassium cations, whereas the second one remains vacant, as shown in Fig. 3. The K$^+$ cation is surrounded by nine oxygen atoms with bond lengths between 2.694 (2) and 3.172 (2) Å.

Bond-valence sum (BVS) calculations (Brown, 1977,1978; Brown & Altermatt, 1985) and charge distribution (CHARDI) (Hoppe *et al.*, 1989) were used to confirm the structure model of β-KCoFe(PO$_4$)$_2$. BVS and CHARDI computations were carried out with *EXPO2014* (Altomare *et al.*, 2013) and *CHARDI2015* (Nespolo & Guillot, 2016), respectively. Table 1 compiles the valences $V_{(i)}$ of cations

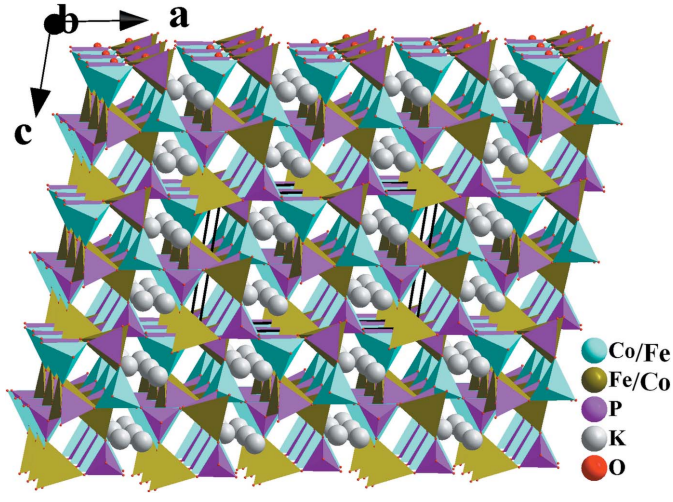

Figure 3
Perspective view of the crystal structure of β-KCoFe(PO$_4$)$_2$ approximately along [010], showing the channels in which the K$^+$ cations are located.

determined with the BVS approach, as well as their corresponding charges $Q_{(i)}$ calculated with the CHARDI concept. The data reveal that the values $Q_{(i)}$ and $V_{(i)}$ are all very close to the corresponding charges $q_{(i)}\times$sof$_{(i)}$ (formal oxidation numbers $q_{(i)}$ weighted by site occupation factors (sof$_{(i)}$). For all cations, the internal criterion $q_{(i)}/Q_{(i)}$ is very close to 1, and the mean absolute percentage deviation (MAPD) that evaluates the agreement between the $q_{(i)}$ and $Q_{(i)}$ charges is 0.3%, confirming the validity of the structural model (Eon & Nespolo, 2015). The global instability index (*GII*) was also used to check the plausibility of the crystal-structure model (Salinas-Sanchez *et al.*, 1992). The *GII* index evaluates the deviation of BVS parameters from the theoretical valence $V_{(i)}$ averaged across all the constitutive atoms of the asymmetric unit. In an unstrained structure, *GII* is less than 0.1 and reaches 0.2 for those with lattice-induced deformations (Adams *et al.*, 2004). For the current crystal structure *GII* amounts to 0.1, indicating its stability.

3. Database survey

The phosphate $KCoFe(PO_4)_2$ crystallizes in two polymorphs in the same crystal system but with different unit-cell parameters and space groups. The α-form of $KCoFe(PO_4)_2$ reported by Badri *et al.* (2019) crystallizes in space group $P2_1/c$ with unit-cell parameters a = 5.148 (1), b = 14.403 (2), c = 9.256 (1) Å, β = 104.87 (2)°. The title compound crystallizes in space group $C2/c$. Whereas the environments around the two *TM* sites are tetrahedral in the title compound, an octahedral coordination is found for one site (Co) in the α-form. The crystal structure of β-$KCoFe(PO_4)_2$ is isotypic with that of $KZnFePO_4)_2$ (Badri *et al.*, 2014), while that of α-$KCoFe(PO_4)_2$ is isotypic with those of $KNiFe(PO_4)_2$ and $KMgFe(PO_4)_2$ (Badri *et al.*, 2015).

4. Synthesis and crystallization

The phosphate β-$KCoFe(PO_4)_2$ was synthesized by mixing cobalt nitrate ($Co(NO_3)_2{\cdot}6H_2O$), iron nitrate [$Fe(NO_3)_3{\cdot}9H_2O$] orthophosphoric acid (H_3PO_4) and potassium nitrate (KNO_3) in molar ratios of 1:1:1:2. The mixture was placed in a small beaker containing distilled water and homogenized for 24 h. After evaporation to dryness, the reaction mixture underwent heat treatments at 573 and 773 K before being brought to fusion for crystal growth at 1223 K, followed by slow cooling. Crystals of purple color and of sufficient size for the analysis by X-ray diffraction were obtained from the final product.

A Quattro ESEM scanning electron microscope (SEM) equipped with an energy dispersive X-ray spectrometer (EDS), operating under 20 kV accelerating voltage, was used for chemical analysis and photographs of the obtained crystals (Fig. 4). Determined mass percentage (+/-3%), calculated mass percentage: K (10.7, 11.4) Fe (12.4, 16.2), Co (13.4, 17.1), P (20.2, 18.0), O (43.3, 37.3)

Table 2
Experimental details.

Crystal data	
Chemical formula	$KCoFe(PO_4)_2$
M_r	343.82
Crystal system, space group	Monoclinic, $C2/c$
Temperature (K)	296
a, b, c (Å)	13.5860 (6), 13.2320 (6), 8.7316 (4)
β (°)	100.335 (2)
V (Å^3)	1544.21 (12)
Z	8
Radiation type	Mo $K\alpha$
μ (mm^{-1})	4.99
Crystal size (mm)	0.36 × 0.27 × 0.15
Data collection	
Diffractometer	Bruker D8 VENTURE Super DUO
Absorption correction	Multi-scan (*SADABS;* Krause *et al.*, 2015)
T_{min}, T_{max}	0.391, 0.747
No. of measured, independent and observed [$I > 2\sigma(I)$] reflections	30042, 3574, 2633
R_{int}	0.068
(sin $\theta/\lambda)_{max}$ (Å^{-1})	0.820
Refinement	
$R[F^2 > 2\sigma(F^2)]$, $wR(F^2)$, S	0.036, 0.088, 1.04
No. of reflections	3574
No. of parameters	118
$\Delta\rho_{max}$, $\Delta\rho_{min}$ (e Å^{-3})	0.98, −0.91

Computer programs: *APEX3* and *SAINT* (Bruker, 2016), *SHELXT2014/7* (Sheldrick, 2015*a*), *SHELXL2018/3* (Sheldrick, 2015*b*), *ORTEP-3 for Windows* (Farrugia, 2012), *DIAMOND* (Brandenburg, 2006) and *publCIF* (Westrip, 2010).

5. Refinement

Crystal data, data collection and structure refinement details are summarized in Table 2. During the refinement, several models were tested, with the best result for a model with occupational disorder of the two *TM* sites. Since the Co:Fe ratio determined from EDS measurements is almost 1:1, this ratio was constrained for the refinement of the individual site occupation, also taking into account full occupancy of both *TM* sites. For the *TM*1 site a ratio of Fe:Co = 0.5725:0.4275 was obtained, for the *TM*2 site a ratio of Co:Fe = 0.5725/0.4275. The maximum and minimum remaining electron density are located at 0.69 Å and 0.31 Å, respectively, from O8.

Acknowledgements

The authors thank the Faculty of Science, Mohammed V University in Rabat, Morocco for the X-ray measurements and the Unit of Support for Technical and Scientific Research (UATRS, CNRST) for the SEM and EDX analysis.

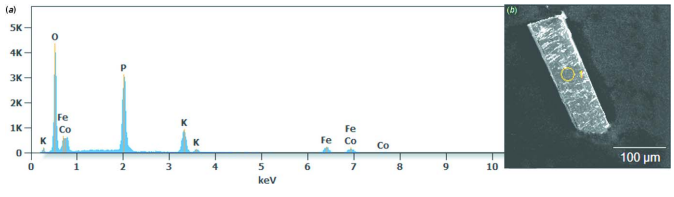

Figure 4
(*a*) EDS spectrum and (*b*) SEM micrographs of the title compound.

References

Adams, S., Moretzki, O. & Canadell, E. (2004). *Solid State Ionics*, **168**, 281–290.

Altomare, A., Cuocci, C., Giacovazzo, C., Moliterni, A., Rizzi, R., Corriero, N. & Falcicchio, A. (2013). *J. Appl. Cryst.* **46**, 1231–1235.

Badri, A., Hidouri, M., López, M. L., Veiga, M. L., Pico, C., Darriet, J. & Ben Amara, M. (2015). *J. Struct. Chem.* **56**, 714–722.

Badri, A., Hidouri, M., Wattiaux, A., López, M. L., Veiga, M. L. & Ben Amara, M. (2014). *Mater. Res. Bull.* **55**, 61–66.

Badri, A., Jabli, M., López, M. L. & Ben Amara, M. (2019). *Inorg. Chem. Commun.* **110**, 107609.

Bautista, F. M., Campelo, J. M., Luna, D., Marinas, J. M., Quirós, R. A. & Romero, A. A. (2007). *Appl. Catal. Environ.* **70**, 611–620.

Benhsina, E., Khmiyas, J., Ouaatta, S., Assani, A., Saadi, M. & El Ammari, L. (2020). *Acta Cryst.* E**76**, 366–369.

Bouraima, A., Assani, A., Saadi, M., Makani, T. & El Ammari, L. (2015). *Acta Cryst.* E**71**, 558–560.

Brandenburg, K. (2006). *DIAMOND*. Crystal Impact GbR, Bonn, Germany.

Brown, I. D. (1977). *Acta Cryst.* B**33**, 1305–1310.

Brown, I. D. (1978). *Chem. Soc. Rev.* **7**, 359–376.

Brown, I. D. & Altermatt, D. (1985). *Acta Cryst.* B**41**, 244–247.

Bruker (2016). *APEX3* and *SAINT*. Bruker AXS Inc., Madison, Wisconsin, USA.

Eon, J.-G. & Nespolo, M. (2015). *Acta Cryst.* B**71**, 34–47.

Farrugia, L. J. (2012). *J. Appl. Cryst.* **45**, 849–854.

Hatert, F., Long, G. J., Hautot, D., Fransolet, A.-M., Delwiche, J., Hubin-Franskin, M. J. & Grandjean, F. (2004). *Phys. Chem. Miner.* **31**, 487–506.

Hoppe, R., Voigt, S., Glaum, H., Kissel, J., Müller, H. P. & Bernet, K. (1989). *J. Less-Common Met.* **156**, 105–122.

Krause, L., Herbst-Irmer, R., Sheldrick, G. M. & Stalke, D. (2015). *J. Appl. Cryst.* **48**, 3–10.

Moore, P. B. & Ito, J. (1979). *Miner. Mag.* **43**, 227–235.

Nespolo, M. & Guillot, B. (2016). *J. Appl. Cryst.* **49**, 317–321.

Ofer, O., Sugiyama, J., Brewer, J. H., Månsson, M., Prša, K., Ansaldo, E. J., Kobayashi, G. & Kanno, R. (2012). *Phys. Procedia*, **30**, 160–163.

Salinas-Sanchez, A., Garcia-Muñoz, J. L., Rodriguez-Carvajal, J., Saez-Puche, R. & Martinez, J. L. (1992). *J. Solid State Chem.* **100**, 201–211.

Sheldrick, G. M. (2015*a*). *Acta Cryst.* A**71**, 3–8.

Sheldrick, G. M. (2015*b*). *Acta Cryst.* C**71**, 3–8.

Shen, Y., Zhao, S., Zhao, B., Ji, C., Li, L., Sun, Z., Hong, M. & Luo, J. (2016). *Inorg. Chem.* **55**, 11626–11629.

Szirtes, L., Riess, L., Megyeri, J. & Kuzmann, E. (2007). *Cent. Eur. J. Chem.* **5**, 516–535.

Trad, K., Carlier, D., Croguennec, L., Wattiaux, A., Ben Amara, M. & Delmas, C. (2010). *Chem. Mater.* **22**, 5554–5562.

Westrip, S. P. (2010). *J. Appl. Cryst.* **43**, 920–925.

Yakubovich, O., Kiriukhina, G., Volkov, A. & Dimitrova, O. (2019). *Acta Cryst.* C**75**, 514–522.

supporting information

Acta Cryst. (2022). E**78**, 746-749 [https://doi.org/10.1107/S2056989022006521]

Crystal growth, structure elucidation and CHARDI/BVS investigations of *β*-$KCoFe(PO_4)_2$

Adam Bouraima, Said Ouaatta, Jamal Khmiyas, Jean Jacques Anguilè, Thomas Makani, Abderrazzak Assani, Mohamed Saadi and Lahcen El Ammari

Computing details

Data collection: *APEX3* (Bruker, 2016); cell refinement: *SAINT* (Bruker, 2016); data reduction: *SAINT* (Bruker, 2016); program(s) used to solve structure: *SHELXT2014/7* (Sheldrick, 2015*a*); program(s) used to refine structure: *SHELXL2018/3* (Sheldrick, 2015*b*); molecular graphics: *ORTEP-3 for Windows* (Farrugia, 2012), *DIAMOND* (Brandenburg, 2006); software used to prepare material for publication: *publCIF* (Westrip, 2010).

Potassium cobalt(II) iron(III) bis(orthophosphate)

Crystal data

$KCoFe(PO_4)_2$
M_r = 343.82
Monoclinic, *C*2/*c*
a = 13.5860 (6) Å
b = 13.2320 (6) Å
c = 8.7316 (4) Å
β = 100.335 (2)°
V = 1544.21 (12) Å^3
Z = 8
F(000) = 1328
D_x = 2.958 Mg m^{-3}
Mo *Kα* radiation, *λ* = 0.71073 Å
Cell parameters from 3574 reflections
θ = 2.2–35.6°
μ = 4.99 mm^{-1}
T = 296 K
Parallelepiped, purple
0.36 × 0.27 × 0.15 mm

Data collection

Bruker D8 VENTURE Super DUO diffractometer
Radiation source: INCOATEC I*μ*S micro-focus source
HELIOS mirror optics monochromator
Detector resolution: 10.4167 pixels mm^{-1}
φ and *ω* scans
Absorption correction: multi-scan (*SADABS;* Krause *et al.*, 2015)
T_{min} = 0.391, T_{max} = 0.747
30042 measured reflections
3574 independent reflections
2633 reflections with $I > 2\sigma(I)$
R_{int} = 0.068
θ_{max} = 35.6°, θ_{min} = 2.2°
h = −13→22
k = −21→21
l = −14→14

Refinement

Refinement on F^2
Least-squares matrix: full
$R[F^2 > 2\sigma(F^2)]$ = 0.036
$wR(F^2)$ = 0.088
S = 1.04
3574 reflections
118 parameters
0 restraints
Primary atom site location: structure-invariant direct methods
Secondary atom site location: difference Fourier map
$w = 1/[\sigma^2(F_o^2) + (0.0363P)^2 + 2.2954P]$ where $P = (F_o^2 + 2F_c^2)/3$

$(\Delta/\sigma)_{max}$ = 0.001
$\Delta\rho_{max}$ = 0.98 e Å^{-3}
$\Delta\rho_{min}$ = −0.91 e Å^{-3}

Special details

Geometry. All esds (except the esd in the dihedral angle between two l.s. planes) are estimated using the full covariance matrix. The cell esds are taken into account individually in the estimation of esds in distances, angles and torsion angles; correlations between esds in cell parameters are only used when they are defined by crystal symmetry. An approximate (isotropic) treatment of cell esds is used for estimating esds involving l.s. planes.

Fractional atomic coordinates and isotropic or equivalent isotropic displacement parameters (Å^2)

	x	*y*	*z*	U_{iso}*/U_{eq}	Occ. (<1)
Fe1	0.37263 (3)	0.06558 (3)	0.61452 (4)	0.01728 (8)	0.5725
Co1	0.37263 (3)	0.06558 (3)	0.61452 (4)	0.01728 (8)	0.4275
Co2	0.07555 (3)	0.11785 (3)	0.04344 (4)	0.01854 (8)	0.5725
Fe2	0.07555 (3)	0.11785 (3)	0.04344 (4)	0.01854 (8)	0.4275
P1	0.42702 (5)	0.14198 (5)	−0.01872 (7)	0.01656 (12)	
P2	0.14880 (5)	0.06783 (5)	0.41434 (7)	0.01769 (12)	
K1	0.31255 (6)	0.25345 (6)	0.27514 (8)	0.03896 (17)	
O1	0.39529 (17)	0.07417 (15)	0.1059 (2)	0.0288 (4)	
O2	0.54020 (16)	0.13970 (16)	−0.0087 (2)	0.0313 (4)	
O3	0.39339 (19)	0.24769 (14)	0.0152 (3)	0.0338 (5)	
O4	0.37488 (19)	0.1089 (2)	−0.1801 (2)	0.0411 (6)	
O5	0.14870 (17)	−0.04718 (15)	0.4068 (2)	0.0312 (4)	
O6	0.1372 (2)	0.11411 (18)	0.2542 (2)	0.0431 (6)	
O7	0.24615 (14)	0.11037 (15)	0.5076 (2)	0.0262 (4)	
O8	0.06510 (17)	0.1025 (2)	0.4989 (3)	0.0475 (7)	

Atomic displacement parameters (Å^2)

	U^{11}	U^{22}	U^{33}	U^{12}	U^{13}	U^{23}
Fe1	0.01435 (16)	0.02100 (16)	0.01659 (14)	0.00191 (12)	0.00307 (11)	−0.00249 (11)
Co1	0.01435 (16)	0.02100 (16)	0.01659 (14)	0.00191 (12)	0.00307 (11)	−0.00249 (11)
Co2	0.01525 (16)	0.02218 (16)	0.01902 (15)	0.00088 (12)	0.00533 (11)	0.00266 (11)
Fe2	0.01525 (16)	0.02218 (16)	0.01902 (15)	0.00088 (12)	0.00533 (11)	0.00266 (11)
P1	0.0185 (3)	0.0157 (2)	0.0169 (2)	0.0005 (2)	0.0071 (2)	−0.00144 (19)
P2	0.0128 (3)	0.0229 (3)	0.0171 (2)	−0.0018 (2)	0.0021 (2)	0.0034 (2)
K1	0.0399 (4)	0.0476 (4)	0.0342 (3)	−0.0028 (3)	0.0197 (3)	−0.0083 (3)
O1	0.0370 (12)	0.0246 (9)	0.0273 (9)	−0.0062 (8)	0.0130 (8)	0.0033 (7)
O2	0.0196 (10)	0.0354 (11)	0.0416 (11)	0.0015 (8)	0.0129 (8)	−0.0039 (9)
O3	0.0478 (14)	0.0212 (9)	0.0388 (11)	0.0109 (8)	0.0254 (10)	0.0033 (8)
O4	0.0407 (14)	0.0625 (16)	0.0201 (9)	−0.0067 (11)	0.0057 (9)	−0.0133 (9)
O5	0.0352 (12)	0.0231 (9)	0.0373 (11)	−0.0083 (8)	0.0116 (9)	0.0011 (8)
O6	0.0560 (16)	0.0449 (13)	0.0247 (10)	−0.0090 (11)	−0.0027 (10)	0.0135 (9)
O7	0.0160 (9)	0.0289 (10)	0.0314 (10)	−0.0003 (7)	−0.0019 (7)	−0.0038 (7)
O8	0.0173 (11)	0.0795 (19)	0.0482 (14)	0.0017 (11)	0.0124 (10)	−0.0163 (13)

Geometric parameters (Å, º)

Fe1/Co1—O4^{i}	1.877 (2)	P2—O5	1.523 (2)
Fe1/Co1—O1^{ii}	1.8783 (19)	P2—O7	1.5308 (19)
Fe1/Co1—O7	1.8972 (19)	P2—O8	1.533 (2)
Fe1/Co1—O2^{iii}	1.900 (2)	K1—O3	2.694 (2)
Co2/Fe2—O6	1.881 (2)	K1—O7^{vii}	2.832 (2)
Co2/Fe2—O8^{iv}	1.891 (2)	K1—O6	2.991 (3)
Co2/Fe2—O3^{v}	1.9191 (19)	K1—O2^{iii}	2.994 (2)
Co2/Fe2—O5^{vi}	1.927 (2)	K1—O8^{vii}	3.019 (3)
P1—O3	1.5172 (19)	K1—O7	3.029 (2)
P1—O4	1.524 (2)	K1—O1	3.110 (2)
P1—O2	1.525 (2)	K1—O4^{v}	3.120 (3)
P1—O1	1.5306 (19)	K1—O5^{viii}	3.172 (2)
P2—O6	1.509 (2)		
O4^{i}—Fe1/Co1—O1^{ii}	111.34 (10)	O7^{vii}—K1—O7	78.19 (6)
O4^{i}—Fe1/Co1—O7	103.45 (10)	O6—K1—O7	47.65 (5)
O1^{ii}—Fe1/Co1—O7	115.36 (9)	O2^{iii}—K1—O7	58.15 (5)
O4^{i}—Fe1/Co1—O2^{iii}	113.73 (10)	O8^{vii}—K1—O7	98.73 (7)
O1^{ii}—Fe1/Co1—O2^{iii}	111.57 (9)	O3—K1—O1	48.80 (5)
O7—Fe1/Co1—O2^{iii}	100.83 (9)	O7^{vii}—K1—O1	166.58 (6)
O6—Co2/Fe2—O8^{iv}	116.47 (11)	O6—K1—O1	81.51 (7)
O6—Co2/Fe2—O3^{v}	101.81 (11)	O2^{iii}—K1—O1	71.69 (6)
O8^{iv}—Co2/Fe2—O3^{v}	108.09 (12)	O8^{vii}—K1—O1	126.06 (7)
O6—Co2/Fe2—O5^{vi}	113.85 (11)	O7—K1—O1	91.04 (5)
O8^{iv}—Co2/Fe2—O5^{vi}	116.25 (11)	O3—K1—O4^{v}	103.24 (7)
O3^{v}—Co2/Fe2—O5^{vi}	97.02 (9)	O7^{vii}—K1—O4^{v}	59.48 (5)
O3—P1—O4	109.84 (14)	O6—K1—O4^{v}	74.98 (7)
O3—P1—O2	110.05 (13)	O2^{iii}—K1—O4^{v}	152.69 (6)
O4—P1—O2	110.14 (13)	O8^{vii}—K1—O4^{v}	97.61 (7)
O3—P1—O1	105.59 (12)	O7—K1—O4^{v}	102.49 (6)
O4—P1—O1	110.20 (13)	O1—K1—O4^{v}	131.79 (6)
O2—P1—O1	110.93 (12)	O3—K1—O5^{viii}	58.15 (5)
O6—P2—O5	111.47 (13)	O7^{vii}—K1—O5^{viii}	84.15 (6)
O6—P2—O7	106.28 (13)	O6—K1—O5^{viii}	133.14 (6)
O5—P2—O7	112.60 (12)	O2^{iii}—K1—O5^{viii}	127.49 (6)
O6—P2—O8	111.23 (16)	O8^{vii}—K1—O5^{viii}	71.38 (7)
O5—P2—O8	108.96 (14)	O7—K1—O5^{viii}	162.10 (6)
O7—P2—O8	106.18 (13)	O1—K1—O5^{viii}	106.85 (5)
O3—K1—O7^{vii}	142.04 (6)	O4^{v}—K1—O5^{viii}	65.29 (6)
O3—K1—O6	111.80 (7)	O3—K1—O3^{v}	77.20 (8)
O7^{vii}—K1—O6	96.69 (7)	O7^{vii}—K1—O3^{v}	102.00 (5)
O3—K1—O2^{iii}	103.65 (7)	O6—K1—O3^{v}	54.25 (5)
O7^{vii}—K1—O2^{iii}	95.61 (6)	O2^{iii}—K1—O3^{v}	149.32 (6)
O6—K1—O2^{iii}	99.16 (6)	O8^{vii}—K1—O3^{v}	140.19 (7)
O3—K1—O8^{vii}	107.98 (8)	O7—K1—O3^{v}	101.04 (5)
O7^{vii}—K1—O8^{vii}	49.37 (6)	O1—K1—O3^{v}	87.81 (5)

O6—K1—O8^{vii}	140.19 (7)	O4^{v}—K1—O3^{v}	44.42 (5)
O2^{iii}—K1—O8^{vii}	69.51 (7)	O5^{viii}—K1—O3^{v}	79.62 (6)
O3—K1—O7	139.67 (6)		

Symmetry codes: (i) *x*, *y*, *z*+1; (ii) *x*, −*y*, *z*+1/2; (iii) −*x*+1, *y*, −*z*+1/2; (iv) −*x*, *y*, −*z*+1/2; (v) −*x*+1/2, −*y*+1/2, −*z*; (vi) *x*, −*y*, *z*−1/2; (vii) −*x*+1/2, −*y*+1/2, −*z*+1; (viii) −*x*+1/2, *y*+1/2, −*z*+1/2.